## **Delocalization Transition of a Disordered Axion Insulator**

Zhi-Da Song, 1,\* Biao Lian, 1 Raquel Queiroz, 2 Roni Ilan, 3 B. Andrei Bernevig, 1,4,5 and Ady Stern, 1 Department of Physics, Princeton University, Princeton, New Jersey 08544, USA
2 Department of Condensed Matter Physics, Weizmann Institute of Science, Rehovot 7610001, Israel
3 Raymond and Beverly Sackler School of Physics and Astronomy, Tel Aviv University, Tel Aviv 69978, Israel
4 Physics Department, Freie Universitat Berlin, Arnimallee 14, 14195 Berlin, Germany
5 Max Planck Institute of Microstructure Physics, 06120 Halle, Germany

(Received 6 November 2020; accepted 30 May 2021; published 29 June 2021)

The axion insulator is a higher-order topological insulator protected by inversion symmetry. We show that, under quenched disorder respecting inversion symmetry *on average*, the topology of the axion insulator stays robust, and an intermediate metallic phase in which states are delocalized is unavoidable at the transition from an axion insulator to a trivial insulator. We derive this conclusion from general arguments, from classical percolation theory, and from the numerical study of a 3D quantum network model simulating a disordered axion insulator through a layer construction. We find the localization length critical exponent near the delocalization transition to be  $\nu = 1.42 \pm 0.12$ . We further show that this delocalization transition is stable even to weak breaking of the average inversion symmetry, up to a critical strength. We also quantitatively map our quantum network model to an effective Hamiltonian and we find its low-energy  $\mathbf{k} \cdot \mathbf{p}$  expansion.

DOI: 10.1103/PhysRevLett.127.016602

Introduction.—Localization of electronic states in disordered systems has been extensively studied in the past decades [1,2]. In particular, studies on the quantum Hall states reveal a profound relation between delocalization and the topology of the electronic state [3–6]. Hence an interesting question is how the localization interplays with the full range of band topologies discovered in the past two decades. For topological insulators [7-13] protected by nonspatial symmetries [14,15], it has been shown that the gapless boundary states are stable against symmetryrespecting disorder [13,16-20], and the phase transition point between phases of different bulk topological numbers has protected extended bulk states at the chemical potential [6,21,22]. Topological states protected by translation [23,24] or mirror [21,25] symmetries are shown to have stable gapless surface states if the crystalline symmetries are respected on average by the disorder. However, such analyses do not explore the effect of disorder on bulk states and do not generalize to the topological states protected by generic crystalline symmetries [26-31], such as higherorder topological insulators [32–39]. Very recently, some numerical studies have shown the robustness of the higherorder topological insulators [40-43], but an understanding of this robustness and of the delocalization transitions of these insulators is still lacking.

In this Letter, we focus on bulk delocalization transitions of a disordered axion insulator [28,44–46], which has been recently identified as a higher-order topological insulator protected by inversion symmetry [32,47–51]. We show that a 3D delocalized metallic phase necessarily arises during

the transition from an axion insulator to a trivial insulator as long as the inversion symmetry is respected (or broken weakly enough) on average. Such a delocalization transition manifests the robustness of the axion insulator topology against disorder.

Layer construction argument.—We consider a 3D crystal with inversion symmetry that maps  $(x, y, z) \rightarrow$ (-x, -y, -z) and translation symmetry that maps  $(x, y, z) \rightarrow (x + t_x, y + t_y, z + t_z),$ with  $t_{x,y,z} \in \mathbb{Z}$ [Fig. 1(c)]. A shifted inversion operation centered at  $(t_x/2, t_y/2, t_z/2)$  consists of the combination of inversion and translation. There are eight shifted inversion centers in each unit cell, corresponding to  $t_{x,y,z} = \{0,1\}$ , respectively. Reference [52] shows that the axion insulator state can be constructed from weakly coupled Chern insulators sublayers [53-56] occupying the inversion centers, where for the A sublayers at  $z = 0, \pm 1, ...$  the Chern number is C=1 and for the B sublayers at  $z=\pm(1/2),\pm(3/2),...$ it is C = -1 [Fig. 1(c)]. The net Chern number in each unit cell is zero. The topology of the axion insulator relies on the fact that one cannot trivialize the construction without breaking inversion symmetry. For example, dimerizing each sublayer A at  $z \in \mathbb{Z}$  with the sublayer B at either  $z + \frac{1}{2}$  or  $z - \frac{1}{2}$  leads to a trivial insulator, but breaks the inversion symmetry [Fig. 1(d)].

Our analysis starts from 2D. We consider a slab made of a finite odd number of layers  $N_z \gg 1$  and a very large number of unit cells in the x, y directions,  $N_{x,y} \gg N_z$ . Topologically the slab is a 2D Chern insulator, say of C = 1. Hence the x - z and y - z sides host chiral modes. Weak disorder

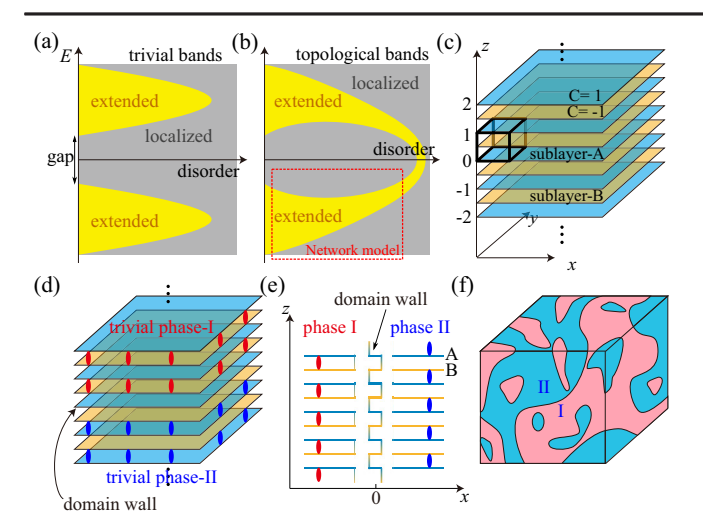


FIG. 1. Localization and band topology. (a),(b) Localized (gray) and delocalized (yellow) regions in the spectrum as a function of disorder for 3D trivial and axion insulators, respectively. (c) Layer construction for the axion insulator, where the black box denotes the 3D unit cell. Sublayers A (blue) and B (orange) are decorated by 2D Chern insulators with Chern numbers C=1,-1, respectively. Each unit cell has eight inversion centers  $(t_x/2,t_y,t_z)$   $(t_{x,y,z}=0,1)$ , all of which lie in a Chern layer. (d) Two possible inversion-breaking dimerized phases (I and II), which are inversion partners. (e) Side view of the domain wall in the xz direction. (f) A disordered axion insulator with random dimerizations, where the red and blue regions represent phases I and II, respectively. The domain walls between phases I and II are Chern layers and host extended states.

localizes all bulk states except states close to two critical energies  $E_{c,1}$ ,  $E_{c,2}$ , one per band. The delocalized states couple the chiral modes on opposite sides, thus allowing a transition between different values of the Chern number. Assuming that the disorder is uniformly distributed within the system, we conclude that the delocalized bulk states are delocalized in all three dimensions in the slab. As disorder gets stronger,  $E_{c,1}$  and  $E_{c,2}$  get closer to one another, until at some critical disorder they become equal, and the system turns trivial at all energies [3–6]. (See Supplemental Material [57] for more discussions.)

Now we approach the 3D limit, making  $N_x$ ,  $N_y$ , and  $N_z$  all very large and comparable to one another. As long as  $N_z$  is odd (required by inversion symmetry) and the chemical potential is tuned properly, the Chern number is C=1, there still is a chiral gapless mode encircling the sample on the side surfaces, and there would still be bulk delocalization transition as a function of energy and disorder. We expect that the critical energies  $E_{c,1}$  and  $E_{c,2}$  develop into two energy regions of extended states, as shown in Fig. 1(b).

This analysis relies on inversion symmetry: If the inversion is broken, e.g., two layers within each unit cell are dimerized, each dimerized pair becomes a trivial insulator, in which disorder localizes all states. The Chern transition is then confined to one unpaired 2D layer.

While this analysis is based on the Chern number that the system carries for an odd  $N_z$ , the thermodynamic 3D limit should not depend on the parity of  $N_z$ . Adding an additional C=-1 layer to the system will not change the localization properties, because the extra layer applies a local perturbation, while the delocalized states are extensive. Thus, the delocalized states occurring at the band gap at a critical disorder strength will remain even in the absence of a Chern number and will signify the transition from an axion to a trivial insulator.

In order to form a physical picture of this transition, we define two inversion-breaking dimerized phases [Fig. 1(d)]: (I) where sublayer A at  $z \in \mathbb{Z}$  couples with sublayer B at  $z-\frac{1}{2}$ , and (II) where sublayer A at  $z \in \mathbb{Z}$  couples with sublayer B at  $z + \frac{1}{2}$ . Phase I and phase II are inversion partners, and the domain wall between them is a Chern insulator layer. The domain wall does not have to be perpendicular to the z direction [see Supplemental Material [57] and Fig. 1(e)]. Inversion-breaking disorders can then be simulated by placing random dimerizations in the 3D bulk, so that the bulk randomly forms phase I and phase II in different regions [Fig. 1(e)]. When the volume fractions of phase I and phase II are equal, we say inversion symmetry is respected on average. We have only considered dimerization disorder for simplicity. More complicated disorder configurations do not change the conclusion [57].

Since each domain wall hosts a 2D Chern insulator with  $C = \pm 1$ , it must host 2D delocalized states at the energy of a delocalization transition. If the domain walls form an infinitely large cluster, the extended states extend over the 3D bulk. Then, when the chemical potential is at the energies of these extended states, a 3D delocalization transition happens to a trivial insulator phase. On the contrary, if the domain walls do not extend to infinity, the disordered axion insulator and trivial insulator would be connected without phase transition. By the classical 3D continuum percolation theory [65], the domain walls extend to infinity if the volume fraction  $p_1$  of phase I (or  $p_2 = 1 - p_1$  of phase II) is between 0.17 and 0.83. Therefore, we expect 3D delocalization transition to exist if inversion symmetry is respected on average  $(p_1 = 0.5)$  or broken weakly enough  $(0.17 < p_1 < 0.83)$ .

Quantum network model.—Our classical percolation argument neglects quantum tunneling between neighboring domain walls. To verify the existence of delocalization transition, we study a disordered 3D quantum network model for the layer-constructed axion insulator, which describes Anderson transition with respect to changing chemical potential. The model includes only one band for each layer and is thus suitable for a transition taking place within that band [Fig. 1(b)]. Its analysis also demonstrates the effect of inversion symmetry breaking on this transition.

In the decoupled layers limit, each sublayer forms a 2D Chalker-Coddington quantum Hall network model [5]

[Figs. 2(a) and 2(b)]. For convenience, here we shift the inversion centers to  $(t_x/2, t_y/2, (1/4) + t_z/2)$   $(t_{x,y,z} = 0, 1)$  such that the Chern layers are in the z = 1/4 and z = 3/4 planes. The blue (orange) and empty regions in sublayer A(B) have C = 1 (C = -1) and C = 0, respectively, while the red lines represent the chiral edge modes. The amplitude  $\psi_i$  of a chiral mode propagating through a bond i gains a (quenched) random propagation phase  $e^{i\phi_i}$ . Two chiral modes are coupled by tunneling at the crossings of the red lines. As shown in Fig. 2(b), the two outgoing modes  $(\psi_2, \psi_4)$  are scattered from the two incoming modes  $(\psi_1, \psi_3)$  as

$$\psi_2 = -t_{A,B}\psi_1 + r_{A,B}\psi_3, \qquad \psi_4 = r_{A,B}\psi_1 + t_{A,B}\psi_3, \quad (1)$$

where  $t_{A,B} = \cos \theta_{A,B}$  and  $r_{A,B} = \sin \theta_{A,B}$  are referred to as the transmission and reflection amplitudes in sublayer A and B, respectively, which we assume are spatially uniform. We choose  $t_{A,B}$  and  $r_{A,B}$  as real numbers because we can absorb their phases into the propagating phases  $\phi_i$ . The sublayers go through a phase transition from  $C = \pm 1$  at  $\pi/4 < \theta_{A,B} \le \pi/2$  to C = 0 at  $0 \le \theta_{A,B} < \pi/4$  [5,57]. At the single-energy  $\theta_{A,B} = \pi/4$ , states in each layer are delocalized.

The decoupled layers limit is inversion symmetric without disorder, i.e., with spatially uniform propagation phases  $\phi_i$ . Looking at the system as 3D, the pillars [Fig. 2(c)] containing the colored regions of sublayers A or B are regions of axion insulators, while the complementary empty regions are trivial insulator regions. We emphasize that there is no explicit relation between the axion or trivial regions and the phase I or phase II shown in Fig. 1. Both the axion regions and trivial regions are centrosymmetric by themselves, while phase I and phase II transform to each other under the inversion. Turning on the disorder (randomness in phases  $\phi_i$ ) breaks inversion symmetry, but preserves it on average when the  $\phi_i$  are uniformly random.

We introduce interlayer scattering nodes at the midpoints of each square, halfway between the intralayer ones, represented by blue vertical lines in Figs. 2(c)–2(e). On each square, there are four scattering nodes. Nodes of the C, D types couple blue layer edge modes to the orange layer edge modes in the layer above, while E, F types couple the blue layer edge modes to the layer below. We parametrize the transmission and reflection amplitudes in the nodes  $t_I = \cos \theta_I$  and  $r_I = \sin \theta_I$  (I = C, D, E, F), respectively. More details of the scattering parameters are given in Fig. S1 in the Supplemental Material [57]. We use four variables  $\mu$ ,  $\gamma$ ,  $\eta$ , and  $\delta$  to parametrize the angles

$$\theta_A = \frac{\pi}{4} + \mu - \eta, \qquad \theta_B = \frac{\pi}{4} + \mu + \eta, \tag{2}$$

$$\theta_C = \theta_D = \gamma(1 - \delta), \qquad \theta_E = \theta_F = \gamma(1 - \delta) + \delta \frac{\pi}{2},$$
(3)

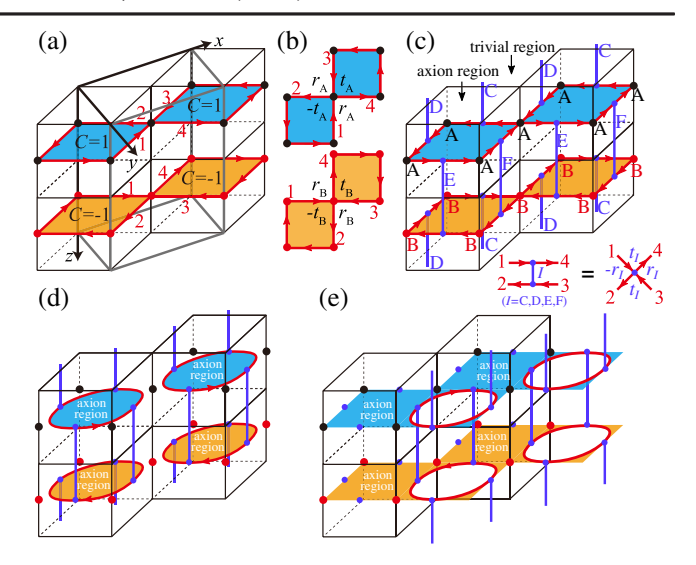


FIG. 2. The quantum network model for the axion insulator. (a) A side view of the 3D system. The blue (orange) regions have a Chern number 1 (-1). The gray box represents the repeating unit. The inversion centers are at  $(t_x/2, t_y/2, 1/4 + t_z/2)$  for  $t_{x,y,z} = 0$ , 1. The red lines with arrows are the chiral modes surrounding the Chern regions. (b) Scatterings at the single-layer level. Here  $t_{A,B}$  and  $r_{A,B}$  are the transmission and reflection amplitudes of the scattering, respectively. (c) Introducing interlayer scatterings. The nodes C, D (E, F) scatter the edge states in the blue layer to the edge states in the orange layer in the above (below). (d),(e) The localized edge states of the Chern regions in the trivial  $(t_{A,B} = 1)$  and axion insulator  $(t_{A,B} = 0)$  limits, respectively.

where  $\mu$  can be interpreted as the chemical potential,  $\eta$  tunes the potential energy difference between two sublayers, and  $\gamma$  and  $\delta$  determine the interlayer couplings. Inversion transforms the nodes C,D to E,F, respectively (Fig. 2); therefore inversion symmetry is broken on average when  $\delta$  is nonzero. We set  $\gamma = \pi/8$  in the rest of this Letter such that the interlayer coupling is weak compared to the intralayer couplings. As explained in the following paragraphs, the insulating limits are independent with  $\gamma$ , hence the choice of  $\gamma$  does not qualitatively change the phase diagram of the quantum network model.

We now study the delocalization transitions with respect to the chemical potential  $(\mu)$ , the potential difference between two layers  $(\eta)$ , and the inversion symmetry breaking  $(\delta)$ . For an inversion symmetric (on average) system  $\eta = \delta = 0$ . The sublayers are either both trivial or both topological. When  $\mu = -\pi/4$ , one has  $t_{A,B} = 1$ , and the chiral modes surrounding the  $C = \pm 1$  regions are closed in each layer but are vertically connected to the closed chiral modes in the nearby layers [Fig. 2(d)]. The axion regions can then be adiabatically shrank to zero, so the 3D bulk is in the trivial insulator phase. When  $\mu = \pi/4$ , the chiral modes flow surrounding the trivial regions  $(t_{A,B} = 0)$  as shown in Fig. 2(e), so the 3D bulk is in the axion insulator phase. In this case, each Chern layer

contributes to a chiral mode on the side surface of the system. Therefore, tuning  $\mu$  from  $-\pi/4$  to  $\pi/4$  tunes the chemical potential from the bottom to the top of the topological bands of the axion insulator [Fig. 1(b)]. In particular, when  $\mu=0$ ,  $\theta_{A,B}$  are equal to  $\pi/4$  and the 3D bulk must be delocalized because the chiral modes form a connected network, corresponding to the region of delocalized states in Fig. 1(b).

In contrast, varying  $\eta$  from 0 to  $\pi/4$  for  $\mu = \delta = 0$ , each sublayer A becomes a trivial insulator ( $\theta_A = 0$ ), while each sublayer B becomes a Chern insulator with C = -1 ( $\theta_B = \pi/2$ ). Therefore,  $\eta$  drives the system into a 3D quantum anomalous Hall (QAH) insulator.

Finally, we consider strong inversion symmetry breaking. When  $\delta = 1$ , there is  $t_C = t_D = 1$ ,  $t_E = t_F = 0$ , and hence a blue layer is decoupled from the orange layer above it, but is fully coupled to the orange layer below it. The 3D network decomposes into disconnected 2D slices in the z direction. Since each slice has a vanishing Chern number, there is no guaranteed delocalized state. Therefore, no delocalization transition with respect to  $\mu$  is expected if  $\delta = 1$ . See the Supplemental Material [57] for more details.

Numerical results.—The localization length of the network model can be computed with a quasi-1D geometry [5,58,59]. Technical details are in the Supplemental Material [57]. A quasi-1D system is always localized, with the localization length depending on the transverse dimension L. The object of interest is the normalized localization length  $\Lambda = \lambda/L$  [58,59]. When  $\Lambda$  is finite or divergent in the  $L \to \infty$  limit, the 3D states are delocalized.

We start with inversion symmetry satisfied on average, i.e.,  $\delta=0$  [ $\delta$  is defined in Eq. (3)]. For  $\eta=0$ , Fig. 3(a) shows  $\Lambda(\mu,L)$  as a function of  $\mu$  and L. At  $\mu=0$ ,  $\Lambda(\mu,L)$  increases with L, which implies 3D delocalized states. In contrast, at  $\mu=\pm\pi/4$ ,  $\Lambda(\mu,L)$  decreases with L and

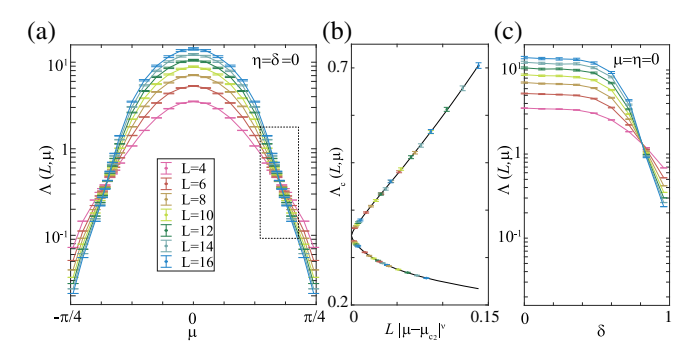


FIG. 3. Numerical results. (a) The normalized localization length  $\Lambda$  of the quasi-1D system is plotted as a function of  $\mu$  at different system sizes (widths) L. The system is delocalized for  $\mu$  between the two Anderson transition points  $\mu_c \approx \pm 0.56$ . (b) shows the one-parameter scaling of the relevant part of  $\Lambda$  around  $\mu \approx 0.56$ . The two branches correspond to  $\mu > 0.56$  and  $\mu < 0.56$ , respectively. (c) The localization transition of  $\Lambda$  due to the inversion symmetry breaking on average, where  $\delta$  tunes the symmetry-breaking strength.

approaches zero as  $L \to \infty$ , implying localized states. As we discussed earlier in Fig. 2,  $\mu = -\pi/4$  and  $\mu = \pi/4$  correspond to the trivial insulator and axion insulator phases, respectively. Figure 3(a) indicates that there is a delocalized metallic phase between them with the two delocalization Anderson transitions happening at  $\mu_c \approx \pm 0.56$ , where  $\Lambda(\mu, L)$ 's for different L's cross each other

On the insulator side of the transitions, the 3D localization length diverges as  $\xi \sim |\mu - \mu_c|^{-\nu}$ , with a universal exponent  $\nu > 0$ . For sufficiently large L,  $\Lambda(\mu, L)$  is subject to the one-parameter scaling of the single-parameter  $L/\xi$  [58,59]. When L is small,  $\Lambda(\mu, L)$  also contains L-dependent irrelevant terms because of the finite-size effect and assumes the following form [66]:

$$\Lambda(\mu, L) = G_0[(\mu - \mu_c)L^{\frac{1}{\nu}}] + L^y G_1[(\mu - \mu_c)L^{\frac{1}{\nu}}]. \tag{4}$$

Here y < 0 is an irrelevant scaling exponent, and  $G_i(x)$  (i=0,1) are undetermined functions that we keep up to the third order. We fit the parameters by the least-square method [57] for the data points in the dashed rectangular in Fig. 3(a). Figure 3(b) shows the relevant part  $\Lambda_c = G_0$  as a function of  $L|\mu - \mu_c|^{\nu}$ . The universal exponent from our fitting is  $\nu = 1.42 \pm 0.12$ , which is close to that of the 3D Anderson transition under magnetic field (where  $\nu$  is found  $1.3 \pm 0.15$  [67],  $1.45 \pm 0.25$  [68],  $1.43 \pm 0.04$  [69], and  $1.443 \pm 0.006$  [70]).

We have theoretically presented arguments that strong inversion symmetry breaking leads to localization and showed that in the network model  $\delta=1$  corresponds to an inversion-broken localized limit. By tuning  $\delta$  in the metal phase at  $\mu=\eta=0$ , we observe an Anderson transition at  $\delta\approx0.81$  to the inversion-broken localized phase [Fig. 3(c)].

Keeping  $\delta=0$  and applying finite-size scaling to non-zero  $\eta$ , which represents the potential energy difference between sublayers A and B, we obtain a phase diagram of Fig. 4(a) in the parameter space of  $\mu$ ,  $\eta$  with inversion symmetry respected on average. A new insulating phase arises near  $\mu=0$ ,  $\eta=\pi/4$ . For a clean system, at  $\mu=0$ ,

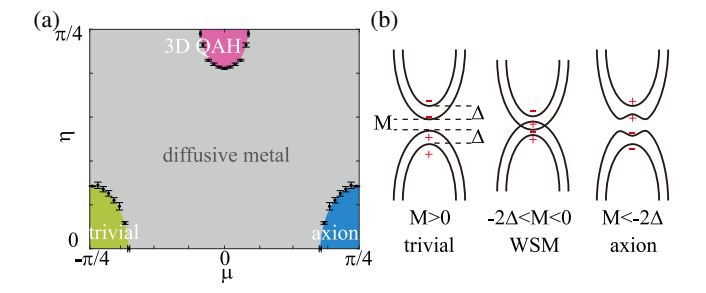


FIG. 4. Disordered topological phases. (a) Phase diagram in the parameter space of  $\mu$  and  $\eta.\delta$  is set to zero. (b) Gap closing transition from trivial insulator to axion insulator. The  $\pm$  symbols represent the parities of the Bloch states.

 $\eta = \pi/4$ , sublayer A is at a C = 0 state and sublayer B is at C = -1; hence this phase is a 3D QAH insulator [71].

Discussion.—We used here  $\mu$  as the transition tuning parameter (Fig. 1). Another possible tuning parameter is the band gap, for which the transitions happen at gap closings that change the topology of the bands [Fig. 4(b)]. We quantitatively map the clean quantum network model to an effective Hamiltonian, where the parameter  $\mu$  plays the role of gap and the diffusive metal in Fig. 4(a) is found to be equivalent to the Weyl semimetal (WSM) [72–76] with disorder [77–79]. See the Supplemental Material [57] for more discussions. We expect the delocalization transitions to be studied in the recently proposed axion insulator materials [49–51,80–85] in the future.

We are grateful to Xiao-Yan Xu and Yuanfeng Xu for useful discussions. B. A. B. and Z.-D. S. were supported by the DOE Award No. DE-SC0016239, the Schmidt Fund for Innovative Research, Simons Investigator No. 404513, and the Packard Foundation. Further support was provided by the NSF-EAGER No. DMR 1643312, NSF-MRSEC No. DMR-1420541, and ONR No. N00014-20-1-2303, and Gordon and Betty Moore Foundation through Grant No. GBMF8685 toward the Princeton theory program. The development of the network model is supported by DOE Award No. DE-SC0016239. R. I. and B. A. B. also acknowledge the support from BSF Israel U.S. foundation No. 2018226. A.S. acknowledges supports from the European Research Council (Project LEGOTOP), the National Science Foundation under Grant No. NSF PHY-1748958, the Israel Science Foundation—Quantum Program, and the RC/Transregio 183 of the Deutsche Forschungsgemeinschaft.

*Note added.*—We are aware of a related work [86] focusing more on the surface delocalization transition. Their results, when overlapped, are consistent with ours.

- \*zhidas@princeton.edu †adiel.stern@weizmann.ac.il
- [1] P. W. Anderson, Absence of diffusion in certain random lattices, Phys. Rev. **109**, 1492 (1958).
- [2] E. Abrahams, 50 Years of Anderson Localization (World Scientific, Singapore, 2010).
- [3] D. E. Khmel'nitskii, Quantization of Hall conductivity, JETP Lett. **38**, 552 (1983).
- [4] H. Levine, S. B. Libby, and A. M. M. Pruisken, Electron Delocalization by a Magnetic Field in Two Dimensions, Phys. Rev. Lett. **51**, 1915 (1983).
- [5] J. T. Chalker and P. D. Coddington, Percolation, quantum tunnelling and the integer Hall effect, J. Phys. C 21, 2665 (1988).
- [6] A. W. W. Ludwig, M. P. A. Fisher, R. Shankar, and G. Grinstein, Integer quantum Hall transition: An alternative approach and exact results, Phys. Rev. B 50, 7526 (1994).

- [7] C. L. Kane and E. J. Mele, Z<sub>2</sub> Topological Order and the Quantum Spin Hall Effect, Phys. Rev. Lett. 95, 146802 (2005)
- [8] B. A. Bernevig, T. L. Hughes, and S.-C. Zhang, Quantum spin Hall effect and topological phase transition in HgTe quantum wells, Science **314**, 1757 (2006).
- [9] M. König, S. Wiedmann, C. Brüne, A. Roth, H. Buhmann, L. W. Molenkamp, X.-L. Qi, and S.-C. Zhang, Quantum spin Hall insulator state in HgTe quantum wells, Science 318, 766 (2007).
- [10] M. Z. Hasan and C. L. Kane, Colloquium: Topological insulators, Rev. Mod. Phys. 82, 3045 (2010).
- [11] X.-L. Qi and S.-C. Zhang, Topological insulators and superconductors, Rev. Mod. Phys. 83, 1057 (2011).
- [12] A. Kitaev, Periodic table for topological insulators and superconductors, AIP Conf. Proc. 1134, 22 (2009).
- [13] S. Ryu, A. P Schnyder, A. Furusaki, and A. W. W. Ludwig, Topological insulators and superconductors: Tenfold way and dimensional hierarchy, New J. Phys. 12, 065010 (2010).
- [14] M. R. Zirnbauer, Riemannian symmetric superspaces and their origin in random-matrix theory, J. Math. Phys. (N.Y.) 37, 4986 (1996).
- [15] A. Altland and M. R. Zirnbauer, Nonstandard symmetry classes in mesoscopic normal-superconducting hybrid structures, Phys. Rev. B **55**, 1142 (1997).
- [16] H.-Z. Lu, J. Shi, and S.-Q. Shen, Competition Between Weak Localization and Antilocalization in Topological Surface States, Phys. Rev. Lett. **107**, 076801 (2011).
- [17] H.-T. He, G. Wang, T. Zhang, I.-K. Sou, G. K. L. Wong, J.-N. Wang, H.-Z. Lu, S.-Q. Shen, and F.-C. Zhang, Impurity Effect on Weak Antilocalization in the Topological Insulator Bi<sub>2</sub>Te<sub>3</sub>, Phys. Rev. Lett. 106, 166805 (2011).
- [18] J. Chen, X. Y. He, K. H. Wu, Z. Q. Ji, L. Lu, J. R. Shi, J. H. Smet, and Y. Q. Li, Tunable surface conductivity in bi<sub>2</sub>se<sub>3</sub> revealed in diffusive electron transport, Phys. Rev. B **83**, 241304(R) (2011).
- [19] M. Liu, J. Zhang, C.-Z. Chang, Z. Zhang, X. Feng, K. Li, K. He, L.-l. Wang, X. Chen, X. Dai, Z. Fang, Q.-K. Xue, X. Ma, and Y. Wang, Crossover between Weak Antilocalization and Weak Localization in a Magnetically Doped Topological Insulator, Phys. Rev. Lett. 108, 036805 (2012).
- [20] J. Wang, B. Lian, and S.-C. Zhang, Universal scaling of the quantum anomalous Hall plateau transition, Phys. Rev. B 89, 085106 (2014).
- [21] I. C. Fulga, B. van Heck, J. M. Edge, and A. R. Akhmerov, Statistical topological insulators, Phys. Rev. B 89, 155424 (2014).
- [22] T. Morimoto, A. Furusaki, and C. Mudry, Anderson localization and the topology of classifying spaces, Phys. Rev. B 91, 235111 (2015).
- [23] Z. Ringel, Y. E. Kraus, and A. Stern, Strong side of weak topological insulators, Phys. Rev. B **86**, 045102 (2012).
- [24] R. S. K. Mong, J. H. Bardarson, and J. E. Moore, Quantum Transport and Two-Parameter Scaling at the Surface of a Weak Topological Insulator, Phys. Rev. Lett. 108, 076804 (2012).
- [25] L. Fu and C. L. Kane, Topology, Delocalization Via Average Symmetry and the Symplectic Anderson Transition, Phys. Rev. Lett. 109, 246605 (2012).

- [26] L. Fu, Topological Crystalline Insulators, Phys. Rev. Lett. 106, 106802 (2011).
- [27] R. S. K. Mong, A. M. Essin, and J. E. Moore, Antiferromagnetic topological insulators, Phys. Rev. B 81, 245209 (2010).
- [28] T. L. Hughes, E. Prodan, and B. A. Bernevig, Inversionsymmetric topological insulators, Phys. Rev. B 83, 245132 (2011).
- [29] R.-J. Slager, A. Mesaros, V. Juričić, and J. Zaanen, The space group classification of topological band-insulators, Nat. Phys. 9, 98 (2013).
- [30] C.-X. Liu, R.-X. Zhang, and B. K. VanLeeuwen, Topological nonsymmorphic crystalline insulators, Phys. Rev. B 90, 085304 (2014).
- [31] C. Fang and L. Fu, New classes of three-dimensional topological crystalline insulators: Nonsymmorphic and magnetic, Phys. Rev. B **91**, 161105(R) (2015).
- [32] F. Zhang, C. L. Kane, and E. J. Mele, Surface State Magnetization and Chiral Edge States on Topological Insulators, Phys. Rev. Lett. 110, 046404 (2013).
- [33] W. A. Benalcazar, B. A. Bernevig, and T. L. Hughes, Quantized electric multipole insulators, Science 357, 61 (2017).
- [34] W. A. Benalcazar, B. A. Bernevig, and T. L. Hughes, Electric multipole moments, topological multipole moment pumping, and chiral hinge states in crystalline insulators, Phys. Rev. B 96, 245115 (2017).
- [35] F. Schindler, A. M. Cook, M. G. Vergniory, Z. Wang, S. S. P. Parkin, B. A. Bernevig, and T. Neupert, Higher-order topological insulators, Sci. Adv. 4, eaat0346 (2018).
- [36] F. Schindler, Z. Wang, M. G. Vergniory, A. M. Cook, A. Murani, S. Sengupta, A. Y. Kasumov, R. Deblock, S. Jeon, I. Drozdov *et al.*, Higher-order topology in bismuth, Nat. Phys. 14, 918 (2018).
- [37] J. Langbehn, Y. Peng, L. Trifunovic, F. von Oppen, and P. W. Brouwer, Reflection-Symmetric Second-Order Topological Insulators and Superconductors, Phys. Rev. Lett. 119, 246401 (2017).
- [38] Z. Song, Z. Fang, and C. Fang, (*d* 2)-Dimensional Edge States of Rotation Symmetry Protected Topological States, Phys. Rev. Lett. **119**, 246402 (2017).
- [39] M. Ezawa, Higher-Order Topological Insulators and Semimetals on the Breathing Kagome and Pyrochlore Lattices, Phys. Rev. Lett. **120**, 026801 (2018).
- [40] Z. Su, Y. Kang, B. Zhang, Z. Zhang, and H. Jiang, Disorder induced phase transition in magnetic higher-order topological insulator: A machine learning study, Chin. Phys. B 28, 117301 (2019).
- [41] H. Araki, T. Mizoguchi, and Y. Hatsugai, Phase diagram of a disordered higher-order topological insulator: A machine learning study, Phys. Rev. B 99, 085406 (2019).
- [42] C. Wang and X. R. Wang, Disorder-induced quantum phase transitions in three-dimensional second-order topological insulators, Phys. Rev. Research **2**, 033521 (2020).
- [43] C.-A. Li, B. Fu, Z.-A. Hu, J. Li, and S.-Q. Shen, Topological Phase Transitions in Disordered Electric Quadrupole Insulators, Phys. Rev. Lett. 125, 166801 (2020).
- [44] A. M. Essin, J. E. Moore, and D. Vanderbilt, Magnetoelectric Polarizability and Axion Electrodynamics in Crystalline Insulators, Phys. Rev. Lett. 102, 146805 (2009).

- [45] R. Li, J. Wang, X.-L. Qi, and S.-C. Zhang, Dynamical axion field in topological magnetic insulators, Nat. Phys. 6, 284 (2010).
- [46] A. M. Turner, Y. Zhang, R. S. K. Mong, and A. Vishwanath, Quantized response and topology of magnetic insulators with inversion symmetry, Phys. Rev. B **85**, 165120 (2012).
- [47] N. Varnava and D. Vanderbilt, Surfaces of axion insulators, Phys. Rev. B 98, 245117 (2018).
- [48] B. J. Wieder and B. A. Bernevig, The axion insulator as a pump of fragile topology, arXiv:1810.02373.
- [49] Y. Xu, Z. Song, Z. Wang, H. Weng, and X. Dai, Higher-Order Topology of the Axion Insulator EuIn<sub>2</sub>As<sub>2</sub>, Phys. Rev. Lett. **122**, 256402 (2019).
- [50] C. Yue, Y. Xu, Z. Song, H. Weng, Y.-M. Lu, C. Fang, and X. Dai, Symmetry-enforced chiral hinge states and surface quantum anomalous Hall effect in the magnetic axion insulator Bi<sub>2-x</sub>Sm<sub>x</sub>Se 3, Nat. Phys. **15**, 577 (2019).
- [51] D. Zhang, M. Shi, T. Zhu, D. Xing, H. Zhang, and J. Wang, Topological Axion States in the Magnetic Insulator MnBi<sub>2</sub>Te<sub>4</sub> with the Quantized Magnetoelectric Effect, Phys. Rev. Lett. 122, 206401 (2019).
- [52] L. Elcoro, B. J. Wieder, Z. Song, Y. Xu, B. Bradlyn, and B. A. Bernevig, Magnetic topological quantum chemistry, arXiv:2010.00598.
- [53] Z. Song, T. Zhang, Z. Fang, and C. Fang, Quantitative mappings between symmetry and topology in solids, Nat. Commun. 9, 3530 (2018).
- [54] Z. Song, S.-J. Huang, Y. Qi, C. Fang, and M. Hermele, Topological states from topological crystals, Sci. Adv. 5, eaax2007 (2019).
- [55] H. Song, S.-J. Huang, L. Fu, and M. Hermele, Topological Phases Protected by Point Group Symmetry, Phys. Rev. X 7, 011020 (2017).
- [56] S.-J. Huang, H. Song, Y.-P. Huang, and M. Hermele, Building crystalline topological phases from lower-dimensional states, Phys. Rev. B **96**, 205106 (2017).
- [57] See Supplemental Material at http://link.aps.org/supplemental/10.1103/PhysRevLett.127.016602 for details about the network model and the mapping from the network model to a low energy **k** · **p** model, which includes Refs. [3–6,20,28,46,52,58–64].
- [58] A. MacKinnon and B. Kramer, One-Parameter Scaling of Localization Length and Conductance in Disordered Systems, Phys. Rev. Lett. 47, 1546 (1981).
- [59] A. MacKinnon and B. Kramer, The scaling theory of electrons in disordered solids: Additional numerical results, Z. Phys. B 53, 1 (1983).
- [60] V. I. Oseledets, A multiplicative ergodic theorem. Characteristic Ljapunov, exponents of dynamical systems, Trudy Moskovskogo Matematicheskogo Obshchestva 19, 179 (1968).
- [61] W. H. Press, Numerical Recipes in Fortran 90: Volume 2, Volume 2 of Fortran Numerical Recipes: The Art of Parallel Scientific Computing (Cambridge University Press, Cambridge, England, 1996).
- [62] L. Fu and C. L. Kane, Topological insulators with inversion symmetry, Phys. Rev. B **76**, 045302 (2007).
- [63] H. Watanabe, H. C. Po, and A. Vishwanath, Structure and topology of band structures in the 1651 magnetic space groups, Sci. Adv. 4, eaat8685 (2018).

- [64] C.-M. Ho and J. T. Chalker, Models for the integer quantum Hall effect: The network model, the Dirac equation, and a tight-binding Hamiltonian, Phys. Rev. B 54, 8708 (1996).
- [65] M. B. Isichenko, Percolation, statistical topography, and transport in random media, Rev. Mod. Phys. **64**, 961 (1992).
- [66] K. Slevin and T. Ohtsuki, Corrections to Scaling at the Anderson Transition, Phys. Rev. Lett. 82, 382 (1999).
- [67] M. Henneke, B. Kramer, and T. Ohtsuki, Anderson transition in a strong magnetic field, Europhys. Lett. 27, 389 (1994).
- [68] J. T. Chalker and A. Dohmen, Three-Dimensional Disordered Conductors in a Strong Magnetic Field: Surface States and Quantum Hall Plateaus, Phys. Rev. Lett. 75, 4496 (1995).
- [69] K. Slevin and T. Ohtsuki, The Anderson Transition: Time Reversal Symmetry and Universality, Phys. Rev. Lett. 78, 4083 (1997).
- [70] K. Slevin and T. Ohtsuki, Estimate of the critical exponent of the anderson transition in the three and four-dimensional unitary universality classes, J. Phys. Soc. Jpn. 85, 104712 (2016).
- [71] R. Yu, W. Zhang, H.-J. Zhang, S.-C. Zhang, X. Dai, and Z. Fang, Quantized anomalous Hall effect in magnetic topological insulators, Science 329, 61 (2010).
- [72] A. A. Burkov and L. Balents, Weyl Semimetal in a Topological Insulator Multilayer, Phys. Rev. Lett. 107, 127205 (2011).
- [73] X. Wan, A. M. Turner, A. Vishwanath, and S. Y. Savrasov, Topological semimetal and Fermi-arc surface states in the electronic structure of pyrochlore iridates, Phys. Rev. B 83, 205101 (2011).
- [74] H. Weng, C. Fang, Z. Fang, B. A. Bernevig, and X. Dai, Weyl Semimetal Phase in Noncentrosymmetric Transition-Metal Monophosphides, Phys. Rev. X 5, 011029 (2015).
- [75] B. Q. Lv, H. M. Weng, B. B. Fu, X. P. Wang, H. Miao, J. Ma, P. Richard, X. C. Huang, L. X. Zhao, G. F. Chen, Z. Fang, X. Dai, T. Qian, and H. Ding, Experimental Discovery of Weyl Semimetal TaAs, Phys. Rev. X 5, 031013 (2015).
- [76] S.-Y. Xu, I. Belopolski, N. Alidoust, M. Neupane, G. Bian, C. Zhang, R. Sankar, G. Chang, Z. Yuan, C.-C. Lee, S.-M. Huang, H. Zheng, J. Ma, D. S. Sanchez, B. Wang, A. Bansil, F. Chou, P. P. Shibayev, H. Lin, S. Jia, and M. Z. Hasan,

- Discovery of a Weyl Fermion semimetal and topological Fermi arcs, Science **349**, 613 (2015).
- [77] K. Kobayashi, T. Ohtsuki, K.-I. Imura, and I. F. Herbut, Density of States Scaling at the Semimetal to Metal Transition in Three Dimensional Topological Insulators, Phys. Rev. Lett. 112, 016402 (2014).
- [78] R. Nandkishore, D. A. Huse, and S. L. Sondhi, Rare region effects dominate weakly disordered three-dimensional dirac points, Phys. Rev. B 89, 245110 (2014).
- [79] J. H. Pixley, D. A. Huse, and S. Das Sarma, Rare-Region-Induced Avoided Quantum Criticality in Disordered Three-Dimensional Dirac and Weyl Semimetals, Phys. Rev. X 6, 021042 (2016).
- [80] M. Mogi, M. Kawamura, A. Tsukazaki, R. Yoshimi, K. S. Takahashi, M. Kawasaki, and Y. Tokura, Tailoring tricolor structure of magnetic topological insulator for robust axion insulator, Sci. Adv. 3, eaao1669 (2017).
- [81] D. Xiao, J. Jiang, J.-H. Shin, W. Wang, F. Wang, Y.-F. Zhao, C. Liu, W. Wu, M. H. W. Chan, N. Samarth, and C.-Z. Chang, Realization of the Axion Insulator State in Quantum Anomalous Hall Sandwich Heterostructures, Phys. Rev. Lett. 120, 056801 (2018).
- [82] J. Li, Y. Li, S. Du, Z. Wang, B.-L. Gu, S.-C. Zhang, K. He, W. Duan, and Y. Xu, Intrinsic magnetic topological insulators in van der Waals layered MnBi<sub>2</sub>Te<sub>4</sub>-family materials, Sci. Adv. 5, eaaw5685 (2019).
- [83] Y. Gong, J. Guo, J. Li, K. Zhu, M. Liao, X. Liu, Q. Zhang, L. Gu, L. Tang, X. Feng, D. Zhang, W. Li, C. Song, L. Wang, P. Yu, X. Chen, Y. Wang, H. Yao, W. Duan, Y. Xu, S.-C. Zhang, X. Ma, Q.-K. Xue, and K. He, Experimental realization of an intrinsic magnetic topological insulator, Chin. Phys. Lett. 36, 076801 (2019).
- [84] Y. Deng, Y. Yu, M. Z. Shi, Z. Guo, Z. Xu, J. Wang, X. H. Chen, and Y. Zhang, Quantum anomalous Hall effect in intrinsic magnetic topological insulator mnbi2te4, Science 367, 895 (2020).
- [85] R.-X. Zhang, F. Wu, and S. D. Sarma, Möbius Insulator and Higher-Order Topology in  $MnBi_{2n}Te_{3n+1}$ , Phys. Rev. Lett. **124**, 136407 (2020).
- [86] H. Li, H. Jiang, C.-Z. Chen, and X. C. Xie, Critical Behavior and Universal Signature of an Axion Insulator State, Phys. Rev. Lett. **126**, 156601 (2021).